

# Effects of SiC Particle Concentration on the Ultrasonic-Assisted Jet Electrodeposited Ni-SiC Nanocoatings

Mengyu Cao, Yuhang Yue, Xue Guo\*, Baojing Wang\*

College of Mechanical Science and Engineering, Northeast Petroleum University, Daqing 163318, China

\*E-mail: [baojwang1234@163.com](mailto:baojwang1234@163.com)

*Received:* 28 September 2021 / *Accepted:* 2 November 2021 / *Published:* 6 December 2021

---

We demonstrate here the use of ultrasonic-assisted jet electrodeposition to prepare abrasive resistant coatings of Ni-SiC on Q235 steel substrate surface. We show that SiC nanoparticle concentration has a profound effect on the morphology and performance of deposited Ni-SiC nanocoatings. We perform a series of physico-chemical characterizations to reveal their structure and morphology to better optimize their abrasion resistance. We show that the SiC contents in the coatings increased first and then decreased as the SiC concentration increased. The ultrasonic-assisted jet deposited Ni-SiC nanocoatings at 7 g/L showed fine grains, smooth and compact microstructure surface, maximum composite amount of SiC nanoparticles, uniform distribution, and no obvious agglomeration. These features results in coatings which possess high microhardness, corrosion resistance and abrasive resistance at the same time.

---

**Keywords:** ultrasonic-assisted jet electrodeposition; Ni-SiC nanocoatings; SiC concentration; abrasive resistance; corrosion resistance

## 1. INTRODUCTION

Nickel-based alloy nanocoatings are widely employed in the chemical, mechanical, aerospace and other fields because of their abrasive resistance, corrosion resistance; and high hardness. Several reports exist on co-deposition of different metals such as nickel, zinc, nickel-tungsten [1, 2] or ceramic particles such as Al<sub>2</sub>O<sub>3</sub> [3], TiO<sub>2</sub> [4], SiC [5] and other metals [6] on the Q235 steel surface for preparing metal matrix composite nanocoatings (MMCNs). The ultrasonic-assisted jet electrodeposition technology is a deposition method with a low cost and fast deposition rate, which can greatly enhance the corrosion resistance and abrasive resistance of a metal matrix [7-9]. The ultrasonic-assisted jet

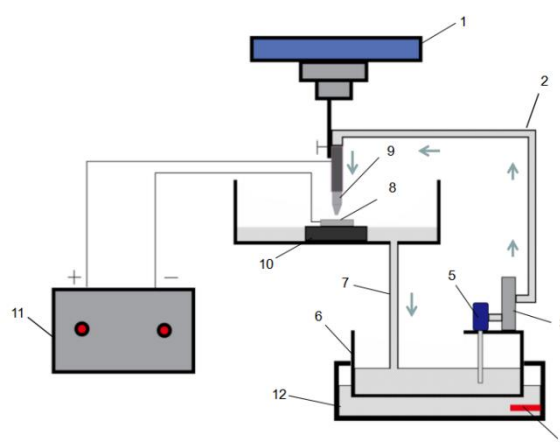
electrodeposition technology uses the anode nozzle which sprays the electrolyte on the cathode workpiece under the ultrasonic conditions. This forms a closed loop between the cathode and anode in the spraying area and completes the electrodeposition of cations on the cathode workpiece [10, 11].

Despite the intense research in this area, at present, the studies on effects of different SiC nanoparticle concentrations on the microstructure, corrosion resistance, and abrasive resistance of ultrasonic-assisted jet electrodeposited Ni-SiC nanocoatings are relatively rare. Therefore, in the present study, we used SiC nanoparticles as the second phase particles for preparing ultrasonic-assisted jet electrodeposited nanocoatings to improve the mechanical properties of Q235 steel substrates. We put emphasis on studying the effect of different SiC concentrations in the bath on the SiC amount, microhardness, corrosion resistance, and abrasive resistance of Ni-SiC nanocoatings.

## 2. EXPERIMENT

### 2.1 Preparation

Fig. 1 shows the schematics of the test device for preparing ultrasonic-assisted jet electrodeposited Ni-SiC nanocoatings. The Q235 steel with a size of 30×40×5 mm was used as cathode. The pure nickel nozzle (nickel content~ 99.98%) was employed as anode. The cathode workpiece was pretreated before the ultrasonic-assisted jet electrodeposition process. Firstly, the cathode was defatted for 10 minutes in a 30 g/L NaOH aqueous solution at 50°C. in the next step, any scales and oxide film was removed by treating the substrates in 30 mL HCl solution (37 wt.%). Finally, the cathode specimen was rinsed with distilled water and dried.



1-servo unite 2-water conduit 3-flowmeter 4-heating rod 5-circulating pump 6-plating bath 7-return pipe 8-Q235 steel matrix 9-nickel nozzle 10-insulated operating table 11-power source 12-ultrasonic generator

**Figure 1.** Schematic diagram of experimental setup

Fig. 2 shows transmission electron microscopy (TEM) image of SiC nanoparticles. The average diameter of the particles was about 50 nm. The electrolyte used for deposition was ultrasonicated for about 1 h to keep the SiC nanoparticles suspended in the solution and to reduce the agglomeration. Cetyltrimethylammonium bromide (CTAB) surfactant was added to the electrolyte (the ratio of surfactant to SiC nanoparticles was 0.1) [12]. The composition of the electrolyte and experimental parameters of ultrasonic-assisted jet electrodeposition process of Ni-SiC nanocoatings are shown in Table 1.

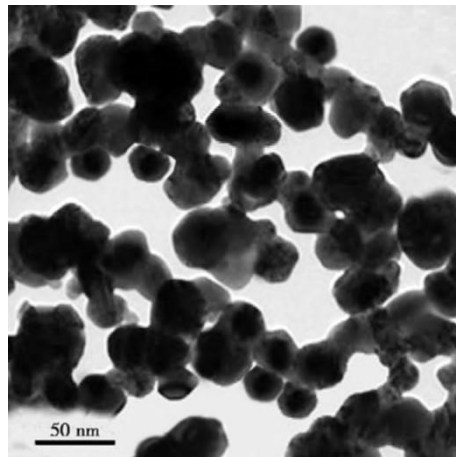


**Figure 2.** TEM image of SiC nanoparticles (Average diameter: 50 nm)

**Table 1.** Composition of electrolyte and process conditions

Composition and process condition	Addition
NiSO <sub>4</sub> ·6H <sub>2</sub> O	140 g/L
NiCl <sub>2</sub> ·6H <sub>2</sub> O	30 g/L
Na <sub>2</sub> WO <sub>4</sub> ·2H <sub>2</sub> O	30 g/L
H <sub>3</sub> C <sub>6</sub> H <sub>5</sub> O <sub>7</sub>	0.1 g/L
SiC nanoparticles	5, 7, 9 g/L
Ultrasonic power	200 W
Current density	2.5 A/dm <sup>2</sup>
pH	4
Temperature	50°C
Time	50 min

## 2.2 Test characterization

The surface morphology and the Si content (wt.%) of the Ni-SiC nanocoatings was measured by S-4800 SEM and EDS, respectively. The amount of SiC nanoparticles in the composites was calculated using the following formula:

$$w(\text{SiC}) = \frac{M(\text{SiC})}{M(\text{Si})} \times w(\text{Si}) \quad (1)$$

Where  $W(\text{SiC})$  is the mass fraction of SiC nanoparticles,  $M(\text{SiC})$  is the molecular weight of SiC,  $M(\text{Si})$  is the molecular weight of Si,  $W(\text{Si})$  is the mass fraction of Si in the Ni-SiC nanocoatings, determined by EDS [13].

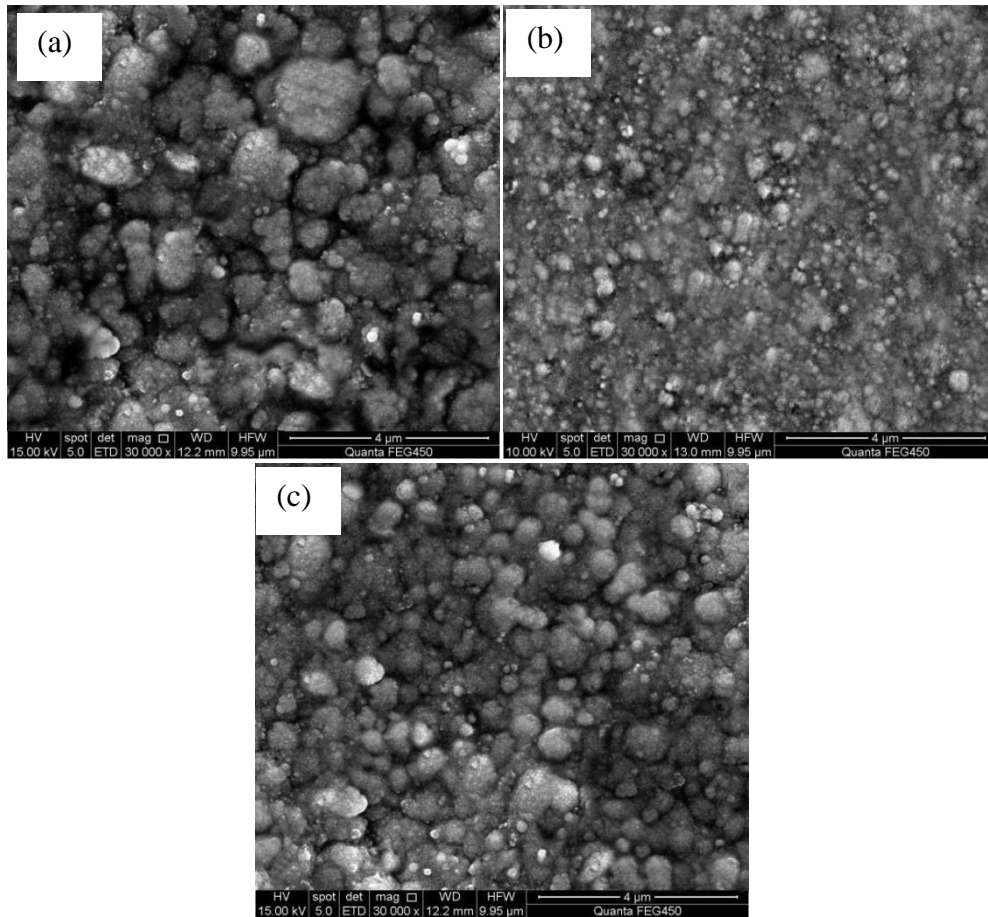
The microhardness of Ni-SiC nanocoatings was determined using a 10 g load and 10 s loading time using a 401MVA microhardness tester. Three independent measurements were performed, average of which was used as final microhardness value. The abrasive resistance and friction coefficient of Ni-SiC nanocoatings was measured by MPX-3 pin-disk in the friction and wear tester at a load of 10 N, 4 mm pin diameter of high carbon steel with a sliding distance of 100 m.

The electrochemical properties of Ni-SiC coating were studied using a three electrode system. A 3.5 wt.% NaCl solution was used as an electrolyte, the deposited Ni-SiC nanocoatings acted as the working electrode (12 mm×12 mm), the saturated calomel electrode (SCE) was used as a reference electrode, and the graphite electrode (CE) acted as an auxiliary electrode. The polarization curves of Ni-SiC nanocoatings were measured using a CS-350 style electrochemical workstation. The scanning rate of anodic polarization and the potential range were 1 mV/s and -0.1~ 0.1V, respectively.

### 3. RESULTS AND DISCUSSION

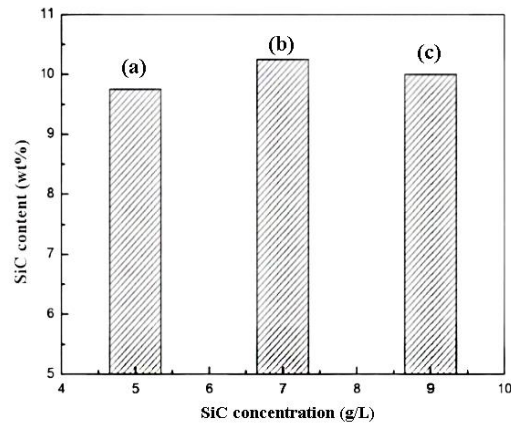
#### 3.1. Surface morphology and microstructure

Fig. 3 displays the SEM images of ultrasonic-assisted jet electrodeposited Ni-SiC nanocoatings produced at different SiC nanoparticle concentrations. As shown in Fig. 3, the grain size of the nanocoatings deposited at 5 g/L is significantly larger than those deposited at 7 and 9 g/L concentrations. When the SiC concentration in the electrolyte increased, the deposition of nickel ions was prohibited because the SiC nanoparticles adsorbed on the activated portion of the substrate surface blocked all the conducting substrate during the deposition process. In addition, high SiC nanoparticle concentration in the electrolyte can provide more nucleation sites on the cathode surface. The microstructure and the surface of Ni-SiC nanocoatings become more compact and smoother when SiC particle content of coatings was increased. Fig. 4(c) reveals that a large number of gaps emerged on the Ni-SiC nanocoating surface fabricated using a 7 g/L concentration. This could be due to agglomeration of SiC caused by high concentration. At the same time, the co-deposition of nickel grains and SiC nanoparticles was not appropriate, which led to weak adhesion of SiC nanoparticles on the cathode surface which were easily washed away during the ultrasonic-assisted jet electrodeposition process. The coatings obtained under these conditions therefore contained a large number of gaps and pinholes [14].



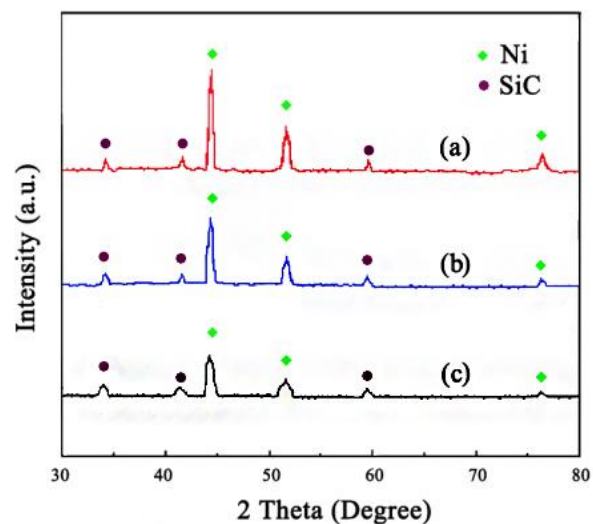
**Figure 3.** SEM images of ultrasonic-assisted jet electrodeposited Ni-SiC nanocoatings produced at: (a) SiC concentration 5 g/L, Ultrasonic power 200 W, Current density 2.5 A/dm<sup>2</sup>, pH 4, Temperature 50 °C; (b) SiC concentration 7 g/L, Ultrasonic power 200 W, Current density 2.5 A/dm<sup>2</sup>, pH 4, Temperature 50 °C; (c) SiC concentration 9 g/L, Ultrasonic power 200 W, Current density 2.5 A/dm<sup>2</sup>, pH 4, Temperature 50 °C.

Fig. 4 presents the relationship between the SiC nanoparticles concentration in the bath and the amount of SiC nanoparticles in Ni-SiC nanocoatings. As can be seen, the SiC content in the film was first increased and then decreased as the SiC nanoparticle concentration increased. Higher SiC nanoparticle concentration led to the increase of SiC nanoparticles around the cathode. This resulted in enhanced deposition of SiC nanoparticles on the cathode surface and thus increased amount of SiC nanoparticles in the composites. The SiC nanoparticle content of the composite coatings decreased after the SiC nanoparticle concentration was increased beyond 7 g/L, which could be due increased collision rate among particles that results in aggravated agglomeration. Some SiC nanoparticles formed large aggregates in the electrolyte which further reduced the adsorption rate of SiC nanoparticles on the coating surface [15, 16]. The SiC nanoparticle content of the coatings manufactured at 7 g/L concentration reached to a maximum value of 10.25 wt.%, which indicates that the best dispersion and highest adsorption rate of SiC nanoparticles occurs at this concentration.



**Figure 4.** Effect of SiC concentration impacted on the SiC content of Ni-SiC nanocoatings produced at: (a) SiC concentration 5 g/L, Ultrasonic power 200 W, Current density 2.5 A/dm<sup>2</sup>, pH 4, Temperature 50°C; (b) SiC concentration 7 g/L, Ultrasonic power 200 W, Current density 2.5 A/dm<sup>2</sup>, pH 4, Temperature 50°C; (c) SiC concentration 9 g/L, Ultrasonic power 200 W, Current density 2.5 A/dm<sup>2</sup>, pH 4, Temperature 50°C.

Fig. 5 shows the XRD patterns of ultrasonic-assisted jet electrodeposited Ni-SiC nanocoatings prepared at different SiC nanoparticle concentrations. The Ni and SiC phases were both present in Ni-SiC nanocoatings deposited at all SiC nanoparticle concentrations.



**Figure 5.** XRD image of Ni-SiC nanocoatings produced at: (a) SiC concentration 5 g/L, Ultrasonic power 200 W, Current density 2.5 A/dm<sup>2</sup>, pH 4, Temperature 50°C; (b) SiC concentration 7 g/L, Ultrasonic power 200 W, Current density 2.5 A/dm<sup>2</sup>, pH 4, Temperature 50°C; (c) SiC concentration 9 g/L, Ultrasonic power 200 W, Current density 2.5 A/dm<sup>2</sup>, pH 4, Temperature 50°C.

Three strong diffraction peaks of nickel grains appeared at  $44.8^\circ$ ,  $52.2^\circ$  and  $76.7^\circ$  corresponding to (111), (200) and (220) crystal planes, respectively. Three strong diffraction patterns of SiC nanoparticle were observed at  $34.2^\circ$ ,  $41.5^\circ$  and  $59.8^\circ$  corresponding to (111), (200) and (220) crystal planes, respectively. It can be seen that the growth orientation of nickel grain changed to (111) crystal plane as the SiC nanoparticle concentration increased. In addition, SiC nanoparticles provide more nucleation sites and thus inhibit the growth of nickel grains along (200) crystal planes.

### 3.2. Microhardness measurements

Fig. 6 displays the average microhardness of Ni-SiC nanocoatings obtained at diverse SiC nanoparticle concentrations. The microhardness increased gradually when the SiC nanoparticle concentration increased from 5 g/L to 7 g/L. The average microhardness of Ni-SiC nanocoatings obtained at 7 g/L reached to a maximum of 820 Hv. The average hardness of Ni-SiC nanocoating decreased after the SiC nanoparticle concentration increased from 7 g/L to 9 g/L. At the optimum SiC nanoparticle concentration, the SiC nanoparticles were uniformly deposited on the substrate surface, which increased the average microhardness of the Ni-SiC nanocoating [17, 18]. However, the high SiC nanoparticle concentration led to the severe agglomeration of the particles, resulting in the decrease of microhardness of the Ni-SiC nanocoatings.

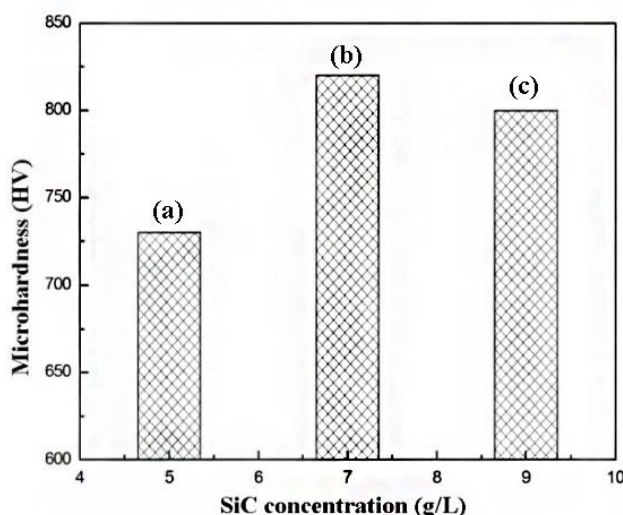


**Figure 6.** The average microhardness values of Ni-SiC nanocoatings deposited at: (a) SiC concentration 5 g/L, Ultrasonic power 200 W, Current density  $2.5 \text{ A/dm}^2$ , pH 4, Temperature  $50^\circ\text{C}$ ; (b) SiC concentration 7 g/L, Ultrasonic power 200 W, Current density  $2.5 \text{ A/dm}^2$ , pH 4, Temperature  $50^\circ\text{C}$ ; (c) SiC concentration 9 g/L, Ultrasonic power 200 W, Current density  $2.5 \text{ A/dm}^2$ , pH 4, Temperature  $50^\circ\text{C}$ .

### 3.3. Abrasive resistance analysis

Fig. 7 shows the friction coefficient and abrasive loss of Ni-SiC nanocoatings obtained at different SiC nanoparticle concentrations. Among the three different nanocoatings, the one prepared at 7 g/L possessed the lowest average friction coefficient of 0.23 and the lowest abrasive loss of 9 mg. The friction coefficient and abrasive loss was inversely proportional to the SiC nanoparticle concentration beyond 7 g/L. Fig. 8 shows SEM images of Ni-SiC nanocoatings prepared at different SiC nanoparticles concentrations. The Ni-SiC nanocoatings surface manufactured at 5 g/L coating showed obvious particle shedding phenomenon, which can be due to the low SiC nanoparticle content of nanocoatings which results in low value of microhardness. The shedding parts further aggravated scratches which emerged on the nanocoatings surface in the process of friction and abrasion. There were obvious grinding marks and slight grains loss emerged on the Ni-SiC nanocoatings surface fabricated at the SiC nanoparticle concentration of 9 g/L.

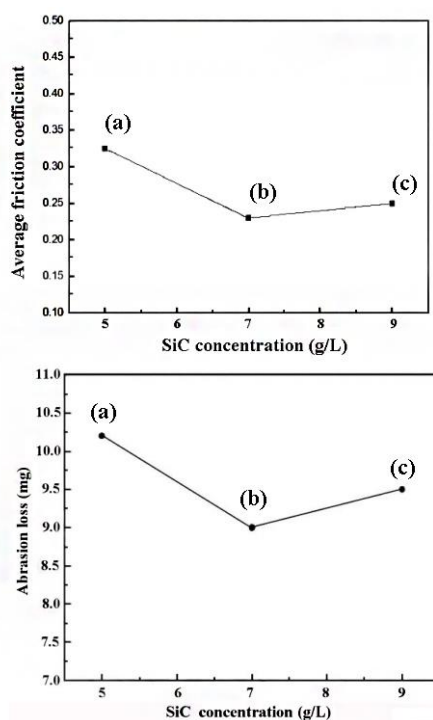


**Figure 7.** Effect of SiC concentrations on the average friction coefficient and abrasion loss of Ni-SiC nanocoatings produced at: (a) SiC concentration 5 g/L, Ultrasonic power 200 W, Current density 2.5 A/dm<sup>2</sup>, pH 4, Temperature 50°C; (b) SiC concentration 7 g/L, Ultrasonic power 200 W, Current density 2.5 A/dm<sup>2</sup>, pH 4, Temperature 50°C; (c) SiC concentration 9 g/L, Ultrasonic power 200 W, Current density 2.5 A/dm<sup>2</sup>, pH 4, Temperature 50°C.

The dispersion and adhesion effect of SiC nanoparticles in the nanocoatings were reduced at high SiC nanoparticle concentration due to their severe agglomeration. The agglomerated SiC nanoparticles chunk of the coating were squeezed out and its hard character further aggravated the abrasion loss of the

coatings [17, 18]. The surface of the Ni-SiC nanocoatings prepared at 7 g/L was smooth and fine. This could be due to the optimum SiC nanoparticle concentration which resulted in uniform dispersion of SiC particles in the film and thus the microhardness and friction coefficient of Ni-SiC nanocoatings prepared at 7 g/L were optimal.

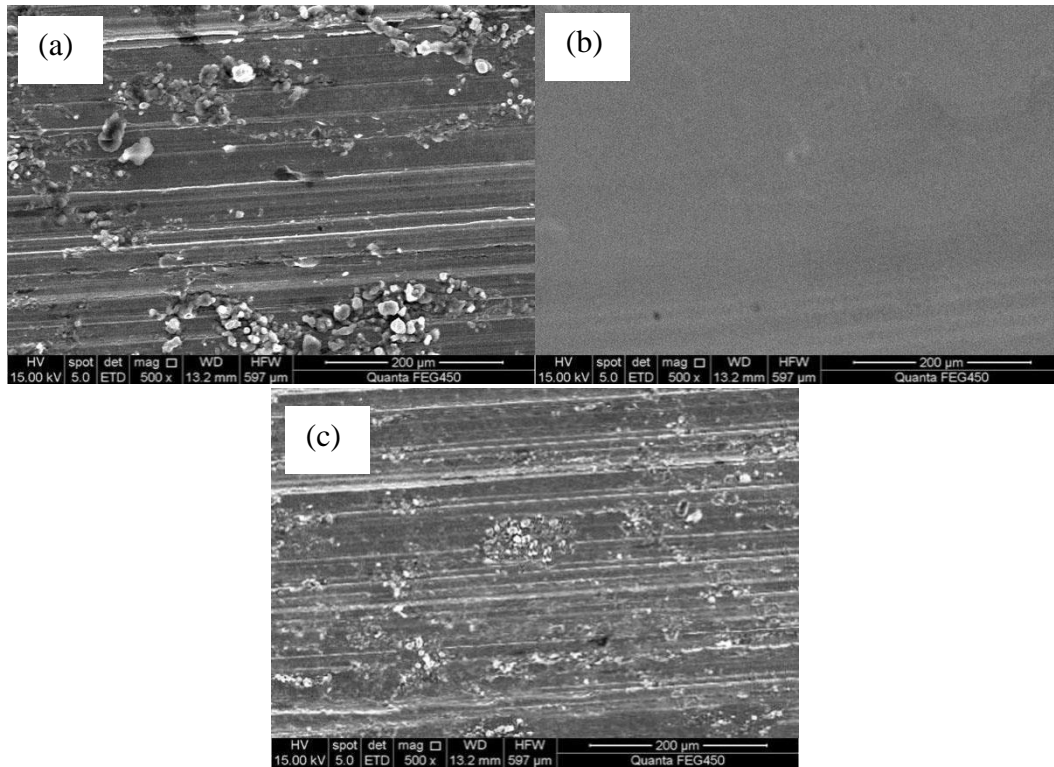


**Figure 8.** SEM image of wear surface of Ni-SiC nanocoating prepared at: (a) SiC concentration 5 g/L, Ultrasonic power 200 W, Current density 2.5 A/dm<sup>2</sup>, pH 4, Temperature 50 °C ; (b) SiC concentration 7 g/L, Ultrasonic power 200 W, Current density 2.5 A/dm<sup>2</sup>, PH 4, Temperature 50 °C ; (c) SiC concentration 9 g/L, Ultrasonic power 200 W, Current density 2.5 A/dm<sup>2</sup>, pH 4, Temperature 50 °C.

### 3.4. Corrosion resistance measurements

Fig. 9 displays the potentiodynamic polarization curves of Ni-SiC nanocoatings, deposited at various SiC nanoparticle concentrations, in 3.5 wt.% NaCl solution. The corrosion potential of Ni-SiC nanocoatings manufactured at 7 g/L was highest (-0.408 V). And the corrosion current density of this coating was about 0.04 μA/mm<sup>2</sup>, which indicated that the coatings had best corrosion resistance.

The higher the SiC nanoparticle concentration, the better corrosion resistance of Ni-SiC nanocoatings before the SiC nanoparticle concentration reached 7g/L. This could be due to excellent chemical stability of SiC material along with adsorbed Ni particles, which further improves the corrosion resistance of the Ni-SiC nanocoatings [19, 20]. Moreover, SiC nanoparticles were conducive to the compactness of nanocoatings preventing the corrosive electrolyte from penetrating into the

nanocoatings. Meanwhile SiC nanoparticles also have the effect of refining and inhibiting the growth nickel grains. On the one hand, dispersion strengthening and fine grain strengthening of SiC nanoparticles in the composites increased lattice dislocations, which hindered lattice growth and improved the stability of Ni-SiC films. On the other hand, the crystal lattice was distorted and deformed by the pinning effect of SiC nanoparticles in the coatings, which resulted in enhancing the grain boundary motion resistance, inhibiting grain growth and refining grain [21, 22]. The corrosion resistance of Ni-SiC nanocoatings prepared at the SiC nanoparticle concentration of 9 g/L was low, due to non-uniform coating of SiC particles which in-turn was due to agglomeration of particles at higher concentrations.

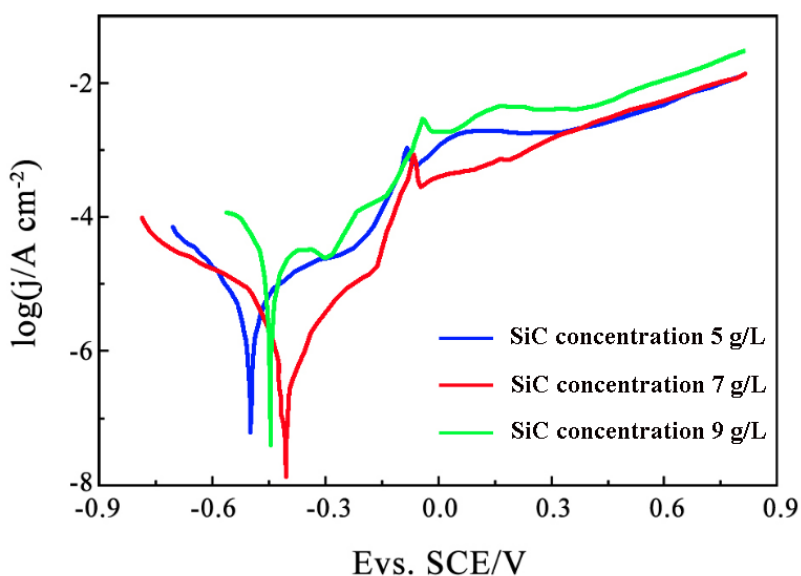


**Figure 9.** Potentiodynamic polarization curves of Ni-SiC nanocoatings produced at: (a) SiC concentration 5 g/L, Ultrasonic power 200 W, Current density 2.5 A/dm<sup>2</sup>, pH 4, Temperature 50 °C; (b) SiC concentration 7 g/L, Ultrasonic power 200 W, Current density 2.5 A/dm<sup>2</sup>, pH 4, Temperature 50 °C; (c) SiC concentration 9 g/L, Ultrasonic power 200 W, Current density 2.5 A/dm<sup>2</sup>, pH 4, Temperature 50 °C.

#### 4. CONCLUSION

(1) The SiC nanoparticle content of Ni-SiC nanocoatings increased first and then decreased when the SiC nanoparticle concentration was increased from 5 to 9 g/L. The SiC nanoparticle content of Ni-SiC nanocoatings produced at 7 g/L was the highest at 10.25 wt.%.

(2) At high SiC nanoparticle concentrations numerous SiC nanoparticles provided more nucleation sites in the process of electrodeposition, which changed the preferred orientation of the nickel crystal grains and inhibiting the growth of (200) crystal plane during the nickel crystallization process.

(3) The microhardness and corrosion current density of Ni-SiC nanocoating prepared at 7 g/L was the highest of 820 Hv and  $0.04 \mu\text{A}/\text{mm}^2$ , respectively. The abrasive loss and friction coefficient of the coatings at this concentration were the lowest of 9 mg and 0.23, respectively.

#### ACKNOWLEDGEMENTS

This work has been supported by the National Natural Science Foundation of China (Granted no. 51974089), Department of Education Innovation Strong School Project (Granted no. 2018KTSCX141), and Daqing Guiding Science and Technology Project (Granted no. Zd-2020-25).

#### References

1. F.F. Xia, C.Y. Li, C.Y. Ma, Q. Li, and H.Y. Xing, *Appl. Surf. Sci.*, 538 (2021) 148139.
2. Z. Wang and Z. Jian, *Corros. Rev.*, 34 (1-2) (2015) 17.
3. D.D. Wang, X.T. Liu, Q. Zhang, Q.W. Li, and D.J. Shen, *Mater. Lett.*, 1-126779 (2021) 129396.
4. I. Nowrouzi, A.K. Manshad, and A.H. Mohammadi, *Fuel*, 259 (2020) 116110.
5. C. Ma, D. Zhao, H. Xia, F. Xia, Z. Ma, and T. Williams, *Int. J. Electrochem. Sci.*, 15 (2020) 4015.
6. C. Ma, X. Guo, J. Leang, and F. Xia, *Ceram. Int.*, 42(8) (2016) 10428.
7. N. Guglielmi, *J. Electrochem. Soc.*, 119 (1972) 1009.
8. F. Xia, Q. Li, C. Ma, W. Liu, and Z. Ma, *Ceram. Int.*, 46 (6) (2020) 7961.
9. F. Xia, Q. Li, C. Ma, and X. Guo, *Ceram. Int.*, 46 (2) (2020) 2500.
10. F. Xia, W. Yue, J. Wang, C. Liu, F. Wang, and Y. Li, *Ceram. Int.*, 41 (9) (2015) 11445.
11. C. Sun, X. Liu, C. Zhou, C. Wang, and H. Cao, *Ceram. Int.*, 45 (1) (2019) 1348.
12. Y. Zhang, L. Wei, H. Zhang, J. Wang, C. Ma, and F. Xu, *J. Mater. Eng. Perform.*, 30 (2021) 6213.
13. X. Shi, M. Kang, X. Fu, and H. Feng, *Coatings*, 11(1) (2021) 72.
14. F.F. Xia, W.C. Jia, C.Y. Ma, R. Yang, Y. Wang, and M. Potts, *Appl. Surf. Sci.*, 434 (2018) 228.
15. C. Li, F. Xia, C. Ma, Q. Li, *J. Mater. Eng. Perform.*, 30(6) (2021) 6336.
16. T. Liu, C. Ma, Q. Li, J. Li, F. Xia, and C. Li, *Int. J. Electrochem. Sci.*, 15 (2020) 12103.
17. C. Ma, W. Yu, M. Jiang, and F. Xia, *Ceram. Int.*, 44 (5) (2018) 5163.
18. J. Zhang, J. Lei, Z. Gu, F. Tantai, and Y. Fang, *Surf. Coat. Technol.*, 393 (2020) 125807.
19. H. Wang, H. Liu, Y. He, C. Ma, and L. Li, *J. Mater. Eng. Perform.*, 30(2) (2021) 1535.
20. H. Zhang, J. Wang, S. Chen, H. Wang, Y. He, and C. Ma, *Ceram. Int.*, 47 (7) (2021) 9437.
21. W. Jiang, L. Shen, M. Qiu, M. Xu, and Z. Tian, *Mater. Res. Express.*, 5(9) (2018) 96407.
22. S. Dehgahi, R. Amini, and M. Alizadeh, *J. Alloy. Compd.*, 692 (2017) 622.